Journal of Materials Chemistry A

Accepted Manuscript

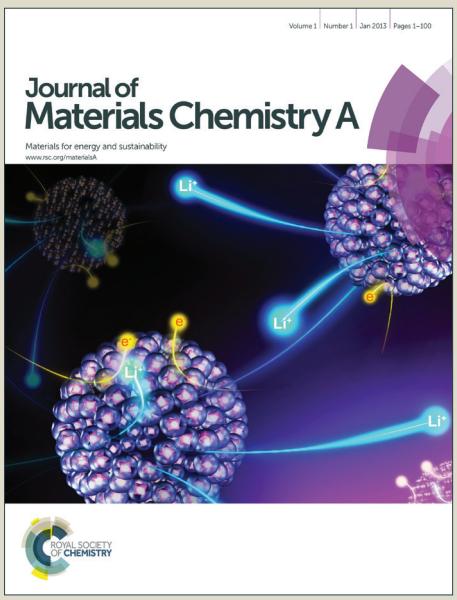

ROYAL SOCIETY OF CHEMISTRY

www.rsc.org/materialsA

Cite this: DOI: 10.1039/c0xx00000x

www.rsc.org/xxxxxx

Communication

Au Nanoparticles on Ultrathin MoS_2 Sheets for Plasmonic Organic Solar Cells

Xi Yang,[‡a] Wenqing Liu,[‡a] Min Xiong,[b] Yingying Zhang,[a] Tao Liang,[a] Jingting Yang,[a] Mingsheng Xu,*[a] Jian Ye*[b] and Hongzheng Chen*[a]

Received (in XXX, XXX) Xth XXXXXXXXX 20XX, Accepted Xth XXXXXXXXX 20XX
DOI: 10.1039/b000000x

A novel hole transport layer (HTL) composed of ultrathin two-dimensional (2D) MoS_2 sheets decorated with 20 nm-sized gold NPs (MoS_2@Au) was developed to make use of plasmonics for organic solar cells (OSCs). Both experimental and theoretical simulation revealed that the device with MoS_2@Au composite as HTL showed the enhanced *Jsc* and efficiency compared to that with MoS_2 alone HTL.

Employment of light trapping based on the localized surface plasmon resonance (LSPR) effect of metallic nanostructures has been proved a promising strategy to improve light harvesting for organic solar cells (OSCs).[1-3] Such efficient light trapping and coupling strategies meet the trade-off of charge transport and light absorption for improving efficiency of thin film photovoltaics.[4] Metallic nanoparticles (NPs) are the most widely utilized sub-wavelength antennas.[5-9] First, the plasmonic near-field can be coupled into the adjacent photoactive materials to effectively increase the cross-section of absorption. Second, metallic NPs can also be used as sub-wavelength scattering elements to prolong the optical path of the incident light within the photoactive layer.[1]

We have previously shown that large-sized metallic NPs can reflect and scatter light better than smaller ones.[10-12] However, small-sized NPs (*i.e.,* <50 nm) are a much better choice by considering the ultra-thin layers of OSC devices.[13] For these small-sized NPs, enhanced light trapping is mainly contributed from the plasmonic near-field enhancement instead of the plasmonic scattering effects.[14] Since the spatial arrangement of enhancing optical absorption is confined in the close vicinity of metal surface,[1] the most straightforward and efficient way is to place metallic NPs in the photoactive

layer,[15-18] where the near-field enhancement of electromagnetic fields from the LSPR can result in enhanced light absorption in active materials surrounding the NPs. Nevertheless, in this approach the possibility of carrier recombination and exciton quenching between the active materials and metallic NPs through the nonradiative energy transfer may also increase.[17,19,20] In addition, the incorporation of NPs into the active layer may induce formation of unfavorable film morphology and disturb phase distribution of donor-acceptor, therefore depressing the exciton separation and charge collection.[15,16] As a result, even though there are numerous methods to successfully embed metallic NPs in interfacial layers (*e. g.,* poly(3,4-ethylenedioxy-thiophene):poly(styrenesulfonate) (PEDOT:PSS)) adjacent to the photoactive layers,[21-25] the direct incorporating of plasmonic NPs into the bulk-heterojunction (BHJ) layer of OSC devices remains an urgent challenge.

Very recently, chemically exfoliated molybdenum disulfide (MoS_2) has been reported to be a novel hole transport material to potentially replace traditional PEDOT:PSS for OSCs.[26] MoS_2 is a layered two-dimensional (2D) transition metal dichalcogenide material. A single layer MoS_2 (thickness of 0.65 nm) consists of two planes of hexagonally arranged S atoms linked to a hexagonal plane of Mo atoms *via* covalent bonds and in its pristine bulk form the individual layers are held together by weak van der Waals forces.[27] The chemical exfoliation method and subsequent solution based thin film formation would facilitate their optoelectronic applications.[28-30] Normally, the thickness of PEDOT:PSS layer used in OSCs is about 40~50 nm, which might mask most plasmonic effects produced by the NPs embedded inside the PEDOT:PSS layer.[31] By contrast, ultrathin MoS_2 layer consisting of atomic thickness of 2D MoS_2 sheets would have potentials to template Au NPs and maximize plasmonic effects of the NPs for OSCs. It would be realizable that such Au NPs on ultrathin 2D MoS_2 layer can touch but do not seriously influence the subsequently deposited BHJ

layer, and thus the plasmonic near-field effects generated by the Au NPs can extend into the BHJ layer efficiently.

Based on this conception, we designed a novel hybrid structure of Au NPs decorated on 2D MoS_2 nanosheets (MoS_2@Au). Such MoS_2@Au composite thin films are supposed to act as a multi-functional hole transport layer (HTL) for OSCs, where the MoS_2 thin film can serve as a hole extraction material facilitating hole collection at the anode and Au NPs function as sub-wavelength antennas, where the plasmonic near-field can be coupled into the photoactive materials to effectively increase the cross-section of absorption. By employing MoS_2@Au HTL into poly[[4,8-bis[(2-ethylhexyl)oxy]benzo[1,2-b:4,5-b′]dithiophene-2,6-diyl][3-fluoro-2-[(2-ethylhexyl)carbonyl]thieno[3,4-b]thiophenediyl]]/[6,6]-phenyl-C71-butyric acid methyl ester (PTB7/PC_{71}BM) blend solar cells, we indeed achieved 15.6% and 17.3% enhancements of the short-circuit photocurrent density (*Jsc*) and the power conversion efficiency (PCE) as compared to the OSCs with a 2D MoS_2 layer but without Au NPs, respectively. The experimental results agree well with the finite-difference time-domain (FDTD) simulation.

MoS_2@Au composite sheets were synthesized by a simple and low-cost solution process on a large scale, where the 20 nm Au NPs (Figure 1a) were introduced on the surface of pre-synthesized MoS_2 nanosheets.[29,30,32] MoS_2 nanosheets were synthesized by a chemical method combining the lithium intercalation and the exfoliation followed by exhaustive dialysis.[33] A majority of the MoS_2 sheets have a thickness of about 1 nm with a lateral size of 200~300 nm, suggesting the monolayer morphology generated by this chemical method (Figure 1b and Figure S1). The high angle annular dark field (HAADF) scanning transmission electron microscopy (STEM) image in Figure 1c reveals the individual Mo and S atoms and their honeycomb arrangement. Compared to the powder X-ray diffraction (XRD) patterns of the bulk MoS_2, only the peak of (002) plane remained while the other

peaks disappeared for the MoS_2 nanosheets (Figure S2), which is mostly due to the fact that the MoS_2 sheets lied on the substrate with preferred orientation and the (002) plane is thermodynamically stable.[34] 20 nm-sized Au NPs were synthesized from Frens method[10] (Figure 1a) and the following decorating onto MoS_2 surface was achieved by simply mixing the MoS_2 and Au NPs colloidal suspensions with different volume ratios. Figures 1d-1f show the TEM images of the obtained MoS_2@Au composites with different Au decoration coverage by changing the mixing ratio, *i.e.,* 5 *vol*%, 12.5 *vol*%, and 20 *vol*%, respectively. A higher magnification TEM image of MoS_2@Au composites with Au decoration of 12.5 *vol*% is shown in Figure S3. It can be clearly observed that the Au NPs on the MoS_2 surface have a uniform size of 20 nm with negligible aggregation; and the quantity of Au NPs on MoS_2 surface is increased with the increase in the mixing ratio. We also find that the Au NPs were only adsorbed on the MoS_2 surface selectively and no individual Au NPs outside the MoS_2 surface were observed, as indicated by the red area in Figure 1d. The decoration is believed to be at both sides of MoS_2 sheets.[32] The decoration might be driven by the interaction between the metal surface and the defects of MoS_2 nanosheets and further investigations of their interactions are needed.[35] The stability of MoS_2@Au composite suspension enables us to use a very simple spin-coating to prepare MoS_2@Au thin film.

Before experimental study, we performed FDTD simulation[36-38] to investigate the LSPR effect of our MoS_2@Au HTL and compared it to the conventional PEDOT:PSS-doping methods (embed Au NPs within the PEDOT:PSS layer) in a conventional OSC device structure. It is known that effectiveness of LSPR is strongly dependent on the size of NPs and the dielectric properties of their surrounding environments.[10] To be consistent with the size of Au NPs used in the present experimental study, we chose 20 nm-sized Au NP as investigated object in the simulation. The calculated extinction (extinction = absorption + scattering) of 20 nm-sized Au NPs in aqueous

solutions is located at 523 nm, identical to the plasmon resonance peak of experimental results (Figures 2a and 2b). However, due to the relatively small size,[10,14] the plasmonic scattering peak for this 20 nm Au NPs is negligible (Figure 2b). Hence, the increase in cross-section of absorption of the photoactive materials with such NPs should mainly be attributed to the plasmonic near-field enhancement.[14] This calculation gives us a preliminary guideline that for small-sized Au NPs light harness strategies should be developed to focus on how to utilize plasmonic near-field enhancement. Hence it is reasonable for the conventional plasmonic device configuration with 20 nm Au NPs integrated in PEDOT:PSS HTL layer that only little photoactive material could be affected by the near-field enhancement because almost all the NPs are wrapped in the 40-50 nm thick PEDOT:PSS layer as illustrated in Figure 2c. In contrast, our MoS_2@Au composite could possibly maximize the near-field enhancement effect because the Au NPs on the ultrathin MoS_2 layer are upwards into the BHJ layer, and thus allow much more photoactive material to surround the metal surface (Figure 2d). To confirm this, we investigated the near-field effect as a function of Au NPs surrounding media and near-field effect distribution directions as below.

It is well known that the plasmonic behaviors of gold nanostructures are strongly dependent on their surrounding media.[39-42] To show the near-field effect of the Au NPs in different environments, the extinction spectrum and near-field distribution of a 20 nm Au NP were simulated by the FDTD method. The simulated extinction cross-section spectra of a 20 nm Au NP in different environments (water, PEDOT:PSS, or PTB7/PC_{71}BM blend) are shown in Figure 3a. The resonance position of 20 nm Au NPs dispersed either in PEDOT:PSS or PTB7/PC_{71}BM blend was red-shifted compared to that in water (λ_{res}=523 nm), which is ascribed to their different dielectric constants.[10] Notably, compared to the relatively small shift in PEDOT:PSS (λ_{res}=542 nm), the resonance position reached 750 nm with an increased extinction cross-section in the whole 500-800 nm range when doping the

Au NPs in PTB7/$PC_{71}BM$ blend. The large wavelength shift led to a much more matched spectral overlap between the resonance wavelength and the absorption of photoactive material (PTB7, with absorption range of 500-750 nm),[17,43-46] suggesting an advantage if 20 nm Au NPs can be incorporated in the active layer. The near-field distributions of a 20 nm Au NP in different environments at corresponding resonance wavelength (water, λ_{res}=523nm; PEDOT:PSS, λ_{res}=542 nm; PTB7/$PC_{71}BM$ blend, λ_{res}=750 nm) are shown in Figures 3b-3d. The incident light was concentrated around the Au NP surface due to the plasmonic effect. The 20 nm Au NP in PTB7/$PC_{71}BM$ blend had a very similar enhanced light intensity to that of PEDOT:PSS ($|E|^2$=94.6 and 95.8, respectively), which was enhanced nearly 100-fold compared with the incident light and more than 4 times that in water ($|E|^2$=22.9). Such high intensity near-field could effectively enhance the absorption of the surrounding photoactive materials.[6]

To further evaluate the near-field distribution at different directions, electric field components along the horizontal (E_x and E_y) and vertical (E_z) direction around Au NP compared with incident light electric field were simulated (Figure 4), where x represents the polarization direction and z represents the polymer growth direction and the light incident direction.[6] We, for the first time, find that the enhanced electric field for 20 nm Au NP is mainly distributed within the horizontal directions while that in the light incident direction is negligible (Figure 4a-i). This phenomenon is of importance for designing near-field enhancement strategies, enhancing in-plane harvest of light with optimized Au NPs coverage on the MoS_2 surface as discussed below. For such small sized NPs of 20 nm, although the photoactive materials could partly fall in the near-field region (10 - 20 nm from the metal surface) of the Au NPs embedded into PEDOT:PSS layer[5,6,21] (Figure 2c), the near-field enhancement at the horizontal direction could not be efficiently coupled into the photoactive layer because of the used thickness of PEDOT:PSS layer. By contrast, our MoS_2@Au composite HTL is

supposed to sufficiently utilize the near-field enhancement produced by the Au NPs upwards into BHJ layer especially at the horizontal direction because of the ultrathin MoS_2 layer (Figure 2d). In addition, we demonstrate that the BHJ layer incorporated by Au NPs on MoS_2 will not disturb much the film morphology and phase distribution. AFM images of BHJ layers on MoS_2 HTL and MoS_2@Au HTL are shown in Figure 2e-f and Figure S4. The similar roughness reveals the morphology and phase distribution of BHJ layer was not altered much.

For a distinct comparison, the calculated plasmonic resonance positions, light electric field intensities, and electric field components along different directions of 20 nm Au NPs in different surrounding media are plotted in Figures 4j-4k. Our simulation results suggest the following advantages of utilizing the plasmonic effects of MoS_2@Au composite as the HTLs for OSCs. First, the device architecture with MoS_2@Au composite HTL could provide the optimized configuration to couple the near-field enhancement into the surrounding photoactive material. The BHJ layer incorporated by plasmonic NPs could be realized without disturbing the film morphology and phase distribution by simply manipulating the interfacial materials. Second, the large range red-shifted resonance position (Figure 4j) is localized in the absorption range of PTB7, maximizing the near-field enhanced absorption of photoactive materials. Third, the enhanced near-field along the horizontal direction could be sufficiently coupled into the active layer.

We fabricated plasmonic OSCs devices with MoS_2@Au composite as HTL (Figure 5a) to verify our anticipation from above simulations. The HTL was formed by sandwiching an ultrathin layer of MoS_2 or MoS_2@Au composite film between the ITO and the PTB7/PC_{71}BM active layer.[47] A layer of poly[(9,9-bis(3′-(N,N-dimethylamino)propyl)-2,7-fluorene)-alt-2,7-(9,9–dioctylfluorene)] (PFN)[38] was deposited on the active layer as electron transport layer to extract electron by the Al cathode.

UV-Vis absorption spectra of PTB7/PC_{71}BM BHJ films before and after the Au NPs incorporated with MoS_2 HTL are presented in Figure 5b. The absorption enhancement after incorporation Au NPs onto MoS_2 sheets is also provided. From Figure 5b, we find that the light absorption in the 500-800 nm region of the BHJ film (PTB7/PC_{71}BM blend) was enhanced and with the largest enhancement at 740 nm by using MoS_2@Au as the HTL with respective to the MoS_2 alone HTL. This largest enhancement location matches well with the plasmon resonance peak (750 nm) of 20 nm Au NPs in PTB7/PC_{71}BM blend simulated by the FDTD method (Figure 3a). The results are in good agreement with the simulation of the environment dependent resonance wavelength shift. And the LSPR effect derived from the MoS_2@Au composite indeed enhanced light absorption of the BHJ layer in OSCs based on PTB7/PC_{71}BM blend.

The performance of OSCs with our MoS_2@Au composite HTL containing different coverages of Au NPs was investigated. Under the 100 mW cm^{-2} illumination (AM 1.5G), the photocurrent-voltage (*J-V*) curves of devices with MoS_2 alone HTL and MoS_2@Au composite HTL are shown in Figure 5c, and their performance are summarized in Table 1. The MoS_2 alone HTL reference device has a PCE of 6.18 % with an open circuit voltage (*Voc*), short-circuit current (*Jsc*), and fill factor (*FF*) of 0.73 V, 13.36 $mAcm^{-2}$, and 0.634, respectively. By decorating the MoS_2 layer with Au NPs, we obtained a maximum *Jsc* (15.44 $mAcm^{-2}$) with a mixing ratio of 12.5 *vol*%. A higher mixing ratio of Au NPs could trade off the near-field plasmonic effect by inducing more recombination centers to depress the carrier collection, resulting in the decreased *Jsc*.[4,10] As a result, with the optimized decoration coverage, we obtained a PCE of 7.25% of the OSCs with MoS_2@Au HTL, showing a 17.3% enhancement compared to the reference device. The unchanged *Voc* and *FF* indicate that the introduction of Au NPs into the HTL did not alter its interfacial property and it remained Ohmic contact with electrode.[10] Thus, the enhanced PCE is mainly due to the increased *Jsc*.

To investigate the origins why the photocurrent increased, external quantum efficiency (EQE) spectra were measured (Figure 5d). Compared to the reference device, the EQE of the device with MoS_2@Au composite HTL was enhanced mostly in the region between 500 and 800 nm, which is consistent well with the enhanced light absorption (Figure 5b). This verifies that the enhanced absorption is the main reason for obtaining higher EQE and PCE.[10-12] Slight enhancement in 350-450 nm regions are observed in both absorption and EQE spectra (Figure 5b and d), illustrating the improved EQE in this region is also from the absorption enhancement.[9,10] Although no obvious peaks are observed in 350-450 nm regions of extinction spectrum of Au NPs, it did have certain values instead of zero. So, the slightly enhanced absorption in this region might be still from the plasmonic effects of Au NPs. Note that the absorption spectra were measured from the structure without the rear electrode of OSCs. Therefore, the 17.3% PCE enhancement was mainly originated from the near-field plasmonic effect of the small Au NPs.

Conclusions

In conclusion, we demonstrated that ultrathin 2D MoS_2 layer can effectively template plasmonic Au NPs to harvest near-field optical absorption for high performance OSCs. The small Au NPs decorated on 2D MoS_2 layer increased the cross-section of absorption of photoactive materials but did not disturb the morphological structures of the photoactive layer. Our simulation and experimental results show that the MoS_2@Au composite HTL for OSCs could more efficiently utilize the enhanced near-field particularly at the horizontal direction. Coupled with the hole extraction capacity of the 2D MoS_2 layer, the plasmonic OSC device with MoS_2@Au HTL containing 12.5*vol*% Au decoration density led to a *Jsc* enhancement of 15.6%, which resulted in a PCE of 7.25% with an enhancement of 17.3% as compared to the device with 2D MoS_2 along HTL. The knowledge developed in our study gives a new insight in utilizing plasmonic near-field

enhancement of small-sized Au NPs and provides a new strategy to integrating Au NPs in BHJ layer for OSCs.

Acknowledgements

This work was supported by the Major State Basic Research Development Program (2014CB643503) and the National Natural Science Foundation of China (Grants 91233114, 51261130582, 50990063, and 21375087). J. Ye gratefully acknowledge the Natural Science Foundation of Shanghai (No. 13ZR1422100) for financial support. M. Xu thanks Zhejiang Provincial Natural Science Foundation of China (Youth Talent Program: R4110030), the Program for New Century Excellent Talents in University (NCET-12-0494), the Research Fund for the Doctoral Program of Higher Education (20130101110123) and the Program for 14th China-Japan S&T Cooperation (2013DFG52800).

Notes and references

[a] State Key Laboratory of Silicon Materials, MOE Key Laboratory of Macromolecular Synthesis and Functionalization, Department of Polymer Science and Engineering, Zhejiang University, Hangzhou 310027, P. R. China
E-mail: hzchen@zju.edu.cn, msxu@zju.edu.cn

[b] Shanghai Engineering Research Center of Medical Device and Technology at Med-X, School of Biomedical Engineering, Shanghai Jiao Tong University, 1954 Huashan Road, Shanghai, 200030, China
E-mail: yejian78@sjtu.edu.cn

†Electronic Supplementary Information (ESI) available: [Experimental section; AFM image and XRD of MoS_2 nanosheets; higher magnification TEM and AFM images of MoS_2@Au composites]. See DOI: 10.1039/b000000x/

‡ These authors contributed equally to this work.

1 H. A. Atwater and A. Polman, *Nature Materials*, 2010, **9**, 205.

2 M. A. Green and S. Pillai, *Nature Photonics*, 2012, **6**, 130.

3 Q. Q. Gan, F. J. Bartoli and Z. H. Kafafi, *Adv. Mater.*, 2013, **25**, 2385.

4 V. E. Ferry, J. N. Munday and H. A. Atwater, *Adv. Mater.*, 2010, **22**, 4794.

5 J. L. Wu, F. C. Chen, Y. S. Hsiao, F. C. Chien, P. L. Chen, C. H. Kuo, M. H. Huang and C. S. Hsu, *ACS Nano*, **2011**, *5*, 959.

6 J. Yang, J. B. You, C. -C. Chen, W. -C. Hsu, H. R. Tan, X. W. Zhang, Z. R. Hong and Y. Yang, *ACS Nano*, 2011, **5**, 6210.

7 L. Y. Lu, Z. Q. Luo, T. Xu and L. P. Yu, *Nano Lett*., 2013, **13**, 59.

8 D. Paz-Soldan, A. Lee, S. M. Thon, M. M. Adachi, H. P. Dong, P. Maraghechi, M. J. Yuan, A. Labelle, S. Hoogland, K. Liu, E. Kumacheva and E. H. Sargent, *Nano Lett*., 2013, **13**, 1502.

9 X. H. Li, W. C. H. Choy, L. J. Huo, F. X. Xie, W. E. I. Sha, B. F. Ding, X. Guo, Y. F. Li, J. H. Hou, J. B. You and Y. Yang, *Adv. Mater.*, 2012, **24**, 3046.

10 X. Yang, C. C. Chueh, C. Z. Li, H. L. Yip, P. P. Yin, H. Z. Chen, W. C. Chen and A. K. Y. Jen, *Adv. Energy Mater*., 2013, **3**, 666.

11 W. F. Fu, X. Q. Chen, X. Yang, L. Wang, Y. Shi, M. M. Shi, H. Y. Li, A. K.-Y. Jen, J. W. Chen, Y. Cao and H. Z. Chen, *Phys. Chem. Chem. Phys*., 2013, **15**, 17105.

12 X. Q. Chen, X. Yang, W. F. Fu, M. S. Xu and H. Z. Chen, *Materials Science and Engineering: B*., 2013, **178**, 53.

13 V. E. Ferry, J. N. Munday and H. A. Atwater, *Adv. Mater*., 2010, **22**, 4794.

14 S. Baek, J. Noh, C. Lee, B. Kim, M. Seo and J. Lee, *Sci Rep*., 2013, **3**, 1726.

15 D. H. Wang, K. H. Park, J. H. Seo, J. Seifter, J. H. Jeon, J. K. Kim, J. H. Park, O. O. Park and A. J. Heeger, *Adv. Energy Mater*., 2011, **1**, 766.

16 D. H. Wang, D. Y. Kim, K. W. Choi, J. H. Seo, S. H. Im, J. H. Park, O. O. Park and A. J. Heeger, *Angew. Chem. Int. Ed*., 2011, **50**, 5519.

17 V. Jankovic, Y. Yang, J. B. You, L. T. Dou, Y. S. Liu, P. Cheung, J. P. Chang and Y. Yang, *ACS Nano*, 2013, **7**, 3815.

18 C. C. D. Wang, W. C. H. Choy, C. H. Duan, D. D. S. Fung, W. E. I. Sha, F. X. Xie, F. Huang and Y. Cao, *J. Mater. Chem*., 2012, **22**, 1206.

19 S. Chang, Q. Li, X. D. Xiao, K. Y. Wong and T. Chen, *Energy Environ. Sci*., 2012, **5**, 9444.

20 W. L. Liu, F. C. Lin, Y. C. Yang, C. H. Huang, S. Gwo, M. H. Huang and J. Huang, *Nanoscale*, 2013, **5**, 7953.

21 F. C. Chen, J. L. Wu, C. L. Lee, Y. Hong, C. H. Kuo and M. H. Huang, *Appl. Phys. Lett.*, 2009,**95**, 013305.

22 D. D. S. Fung, L. F. Qiao, W. C. H. Choy, C. D. Wang, W. E. I. Sha, F. X. Xie and S. L. He, *J. Mater. Chem*., 2011, **21**, 16349.

23 D. Zhang, W. C. H. Choy, F. X. Xie, W. E. I. Sha, X. C. Li, B. F. Ding, K. Zhang, F. Huang and Y. Cao, *Adv. Funct. Mater.* **2013**, *23*, 4255.

24 B. Niesen, B. P. Rand, P. V. Dorpe, D. Cheyns, L. M. Tong, A. Dmitriev and P. Heremans, *Adv. Energy Mater*., 2013, **3**, 145.

25 J. Chen, H. Wu, Y. Chiu and W. Chen, *Adv. Energy Mater*., Doi:10.1002/aenm.201301665.

26 X. Gu, W. Cui, H. Li, Z. W. Wu, Z. Y. Zeng, S. -T. Lee, H. Zhang and B. Q. Sun, *Adv. Energy Mater*., 2013, **3**, 1262.

27 M. S. Xu, T. Liang, M. M. Shi and H. Z. Chen, *Chem. Rev*., 2013, **113**, 3766.

28 X. Yang, W. F. Fu, W. Q. Liu, J. H. Hong, Y. Cai, C. H. Jin, M. S. Xu, H. B. Wang, D. R. Yang and H. Z. Chen, *J. Mater. Chem. A*, 2014, *2*, 7727.

29 G. Q. Fan, Q. Q. Zhuo, J. J. Zhu, Z. Q. Xu, P. P. Cheng, Y. Q. Li, X. H. Sun, S. Lee and J. X. Tang, *J. Mater. Chem*., 2012, **22**, 15614.

30 M. K. Chuang, S. Lin, F. Chen, C. Chu and C. Hsu, *Nanoscale*, 2014, **6**, 1573.

31 H. Choi, J. Lee, S. Ko, J. Jung, H. Park, S. Yoo, O. Park, J. Jeong, S. Park and J. Y. Kim, *Nano Lett*., 2013, **13**, 2204.

32 X. Yang, M. S. Xu, W. M. Qiu, X. Q. Chen, M. Deng, J. L. Zhang, H. Iwai, E. Watanabe and H. Z. Chen, *J. Mater. Chem*., 2011, **21**, 8096.

33 G. Eda, H. Yamaguchi, D. Voiry, T. Fujita, M. W. Chen and M. Chhowalla, *Nano Lett*., 2011, **11**, 5111.

34 Z. Y. Zeng, Z. Y. Yin, X. Huang, H. Li, Q. Y. He, G. Lu, F. Boey and H. Zhang, *Angew. Chem. Int. Ed*., 2011, **50**, 11093.

35 Y. Shi, J. Huang, L. Jin, Y.Hsu, S. F. Yu, L. Li and H. Y. Yang, *Sci Rep*., 2013, **3**, 1839

36 E. D. Palik, *Handbook of Optical Constants of Solids*, Academic Press, Orlando, FL, 1985.

37 H. Hoppe, N. Sariciftci and D. Meissner, *Molecular Crystals and Liquid Crystals*, 2002, **385**, 113.

38 Z. He, C. Zhong, S. Su, M. Xu, H. Wu and Y. Cao, *Nature Photonics*, 2012, **6**, 591.

39 J. Ye and P. Van Dorpe, *Nanoscale*, 2012, **4**, 7205.

40 S. Mazzucco, N. Geuquet, J. Ye, O. Stéphan, W. V. Roy, P. V. Dorpe, L. Henrard and M. Kociak, *Nano Lett*., 2012, **12**, 1288.

41 F. F. Wen, J. Ye, N. Liu, P. V. Dorpe, P. Nordlander and N. J. Halas, *Nano Lett*., 2012, **12**, 5020.

42 C. J. Huang, J. Ye, S. Wang, T. Stakenborg and L. Lagae, *Appl. Phys. Lett*., 2012, **100**, 173114.

43 X. N. Dang, J. F. Qi, M. T. Klug, P. Chen, D. S. Yun, N. X. Fang, P. T. Hammond and A. M. Belcher, *Nano Lett*., 2013, **13**, 637.

44 X. Chen, B. H. Jia, J. K. Saha, B. Y. Cai, N. Stokes, Q. Qiao, Y. Q. Wang, Z. R. Shi and M. Gu, *Nano Lett*., 2012, **12**, 2187.

45 Q. Xu, F. Liu, Y. X. Liu, K. Y. Cui, X. Feng, W. Zhang and Y. D. Huang, *Sci Rep*., 2013, **3**, 2112.

46 Y. S. Hsiao, S. Charan, F. Y. Wu, F. C. Chien, C. W. Chu, P. L. Chen and F. C. Chen, *J. Phys. Chem. C*, 2012, **116**, 20731.

47 Y. Y. Liang, Z. Xu, J. B. Xia, S. Tsai, Y. Wu, G. Li, C. Ray and L. P. Yu, *Adv. Mater*., 2010, **22**, 135.

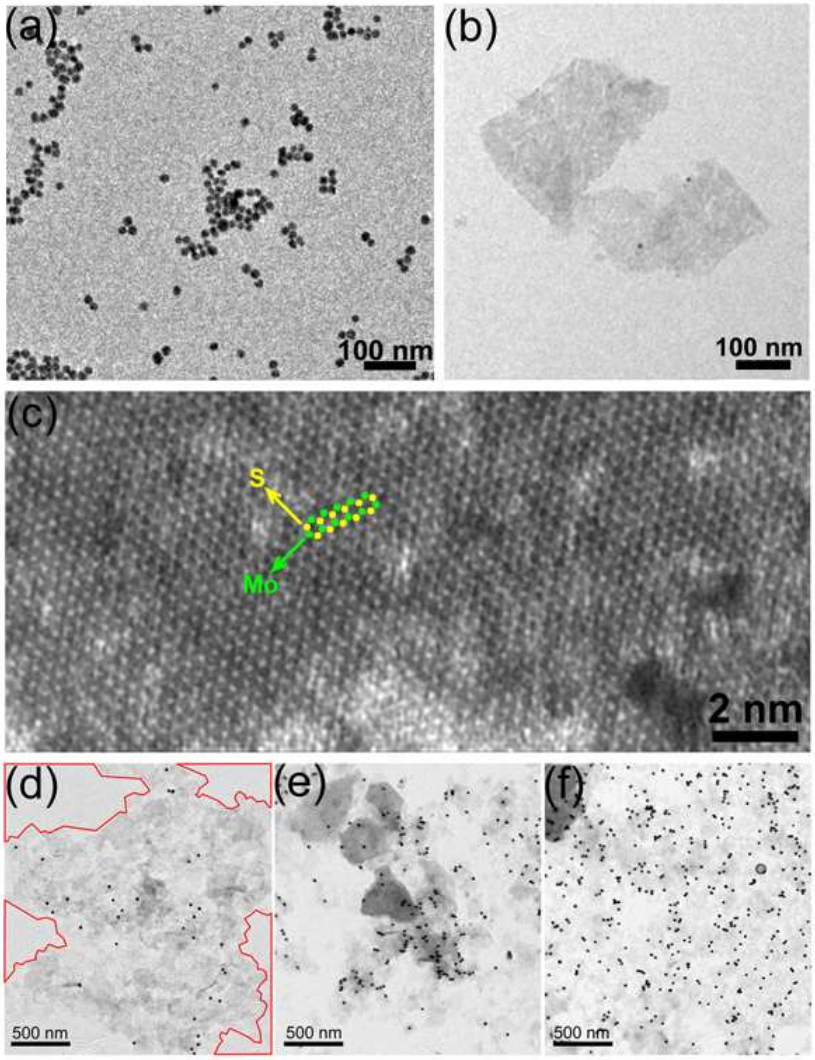

Figure 1. (a) TEM image of 20 nm Au NPs. TEM (b) and HAADF STEM (c) images of chemically exfoliated MoS_2 nanosheets. The HAADF STEM image shows individual Mo and S atoms (represented by green and yellow balls in the image, respectively) and their honeycomb arrangement for the MoS_2 nanosheets. TEM images of MoS_2@Au composites with increased Au NPs decoration coverage obtained by adjusting the mixing ratio: (d) 5 *vol*%, (e) 12.5 *vol*%, and (f) 20 *vol*%. The Au NPs were only adsorbed on the MoS_2 surface selectively and no individual Au NPs outside the MoS_2 surface were observed, as indicated by the red area in Figure 1d.

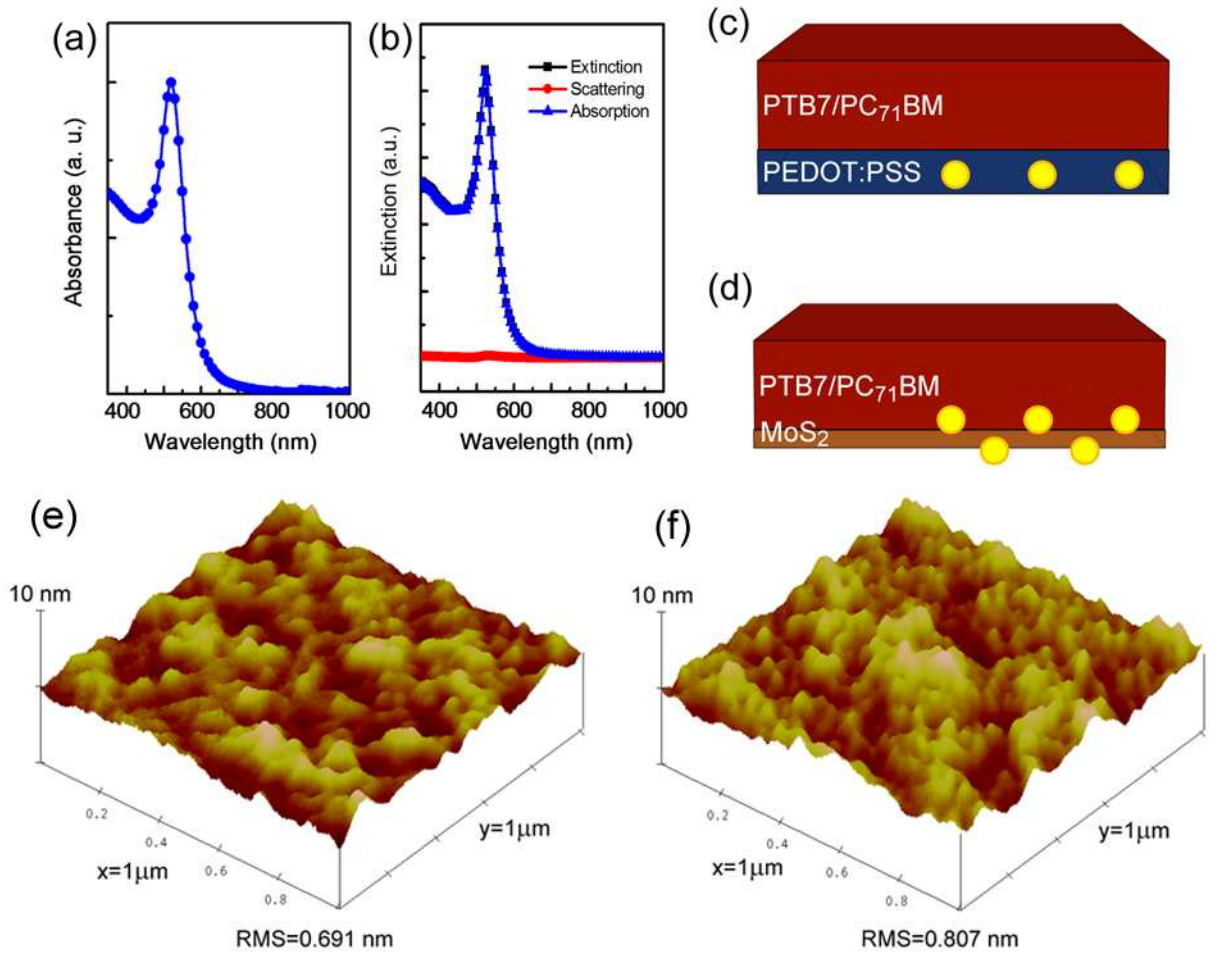

Figure 2. (a) Absorption spectrum of synthesized 20 nm Au NPs in water. (b) The calculated extinction spectrum of 20 nm Au NPs in water. OSC device BHJ geometries with different hole transporting layers: (c) PEDOT:PSS incorporated with 20 nm Au NPs, where the 40 nm thick PEDOT:PSS keep most of the Au NPs inside the interfacial layer. (d) MoS_2@Au, where the Au NPs can be embedded upwards into the upper active layer, providing the optimized configuration to couple the near-field enhancement to the surrounding photoactive materials without disturbing much the film morphology and phase distribution by simply manipulating the interfacial materials. Three-dimensional topography images of BHJ layer on (e) MoS_2 and (f) MoS_2@Au.

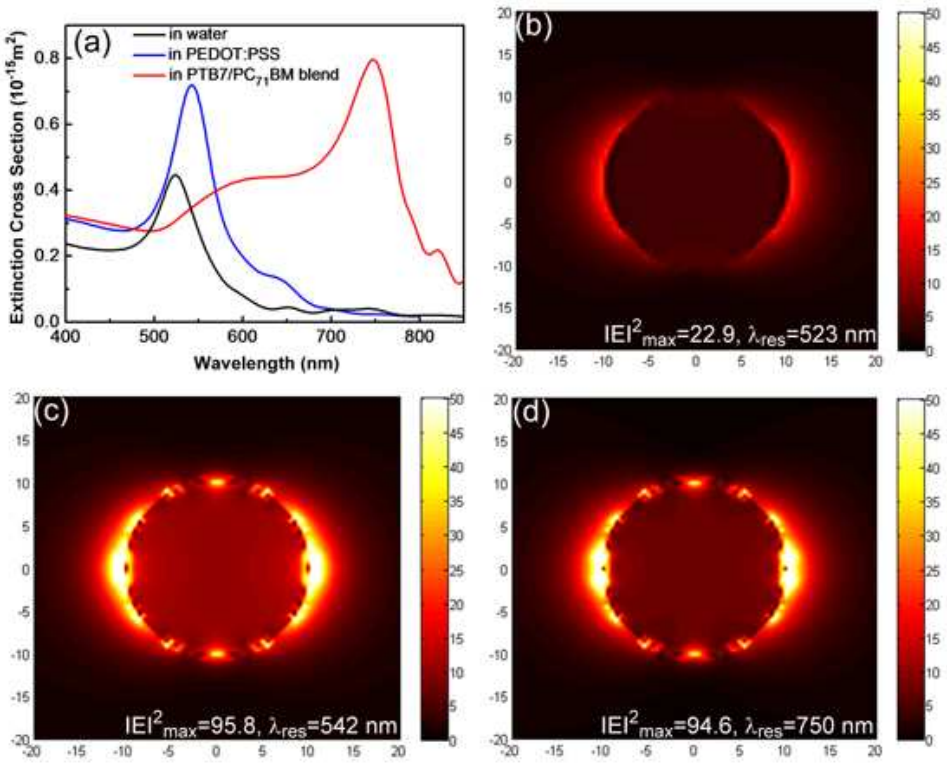

Figure 3. (a) Simulated extinction spectra of isolated Au NPs in water, PEDOT:PSS and PTB7/PC_{71}BM blend. Simulated electric field ($|E|^2$) distribution around Au NP compared with incident light electric field in (b) water, (c) PEDOT:PSS, and (d) PTB7/PC_{71}BM blend. The 20 nm Au NP in PTB7/PC_{71}BM blend has a very similar enhanced light intensity to that of PEDOT:PSS ($|E|^2$=94.6 and 95.8, respectively), which is enhanced nearly 100-fold compared with the incident light and is more than 4 times that in water ($|E|^2$=22.9).

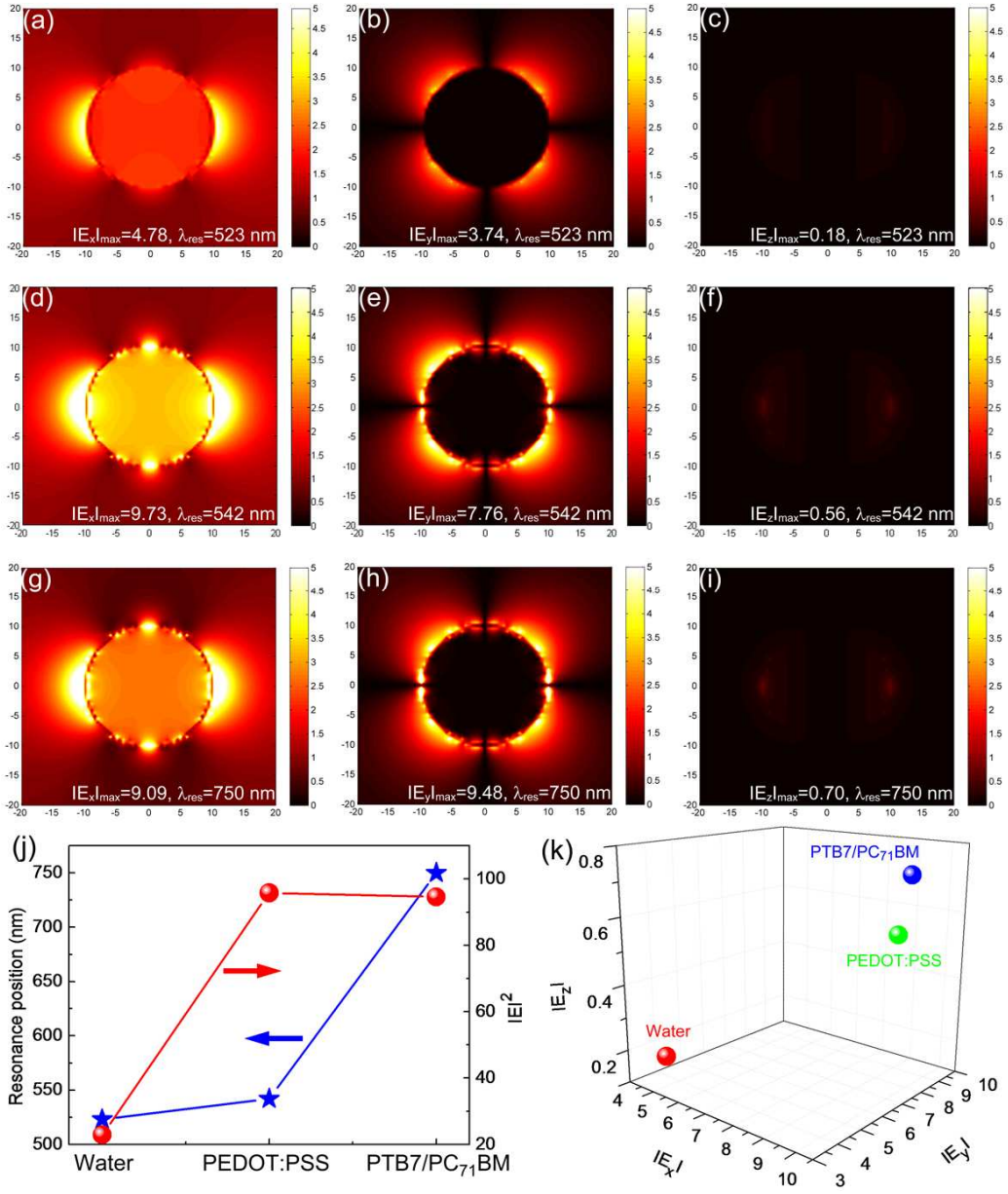

Figure 4. Electric field distribution along the horizontal (E_x and E_y) and vertical (E_z) direction around 20 nm Au NP compared with incident light electric field in different environments: (a-c) water; (d-f) PEDOT:PSS; (g-i) PTB7/PC_{71}BM blend. (j) Calculated resonance position and electric field intensity ($|E|^2$) in different surrounding medium. Au NP in PTB7/PC_{71}BM blend has a significantly red-shifted resonance position and enhanced electric field intensity. (k) Calculated electric field intensity along different directions in different surrounding medium.

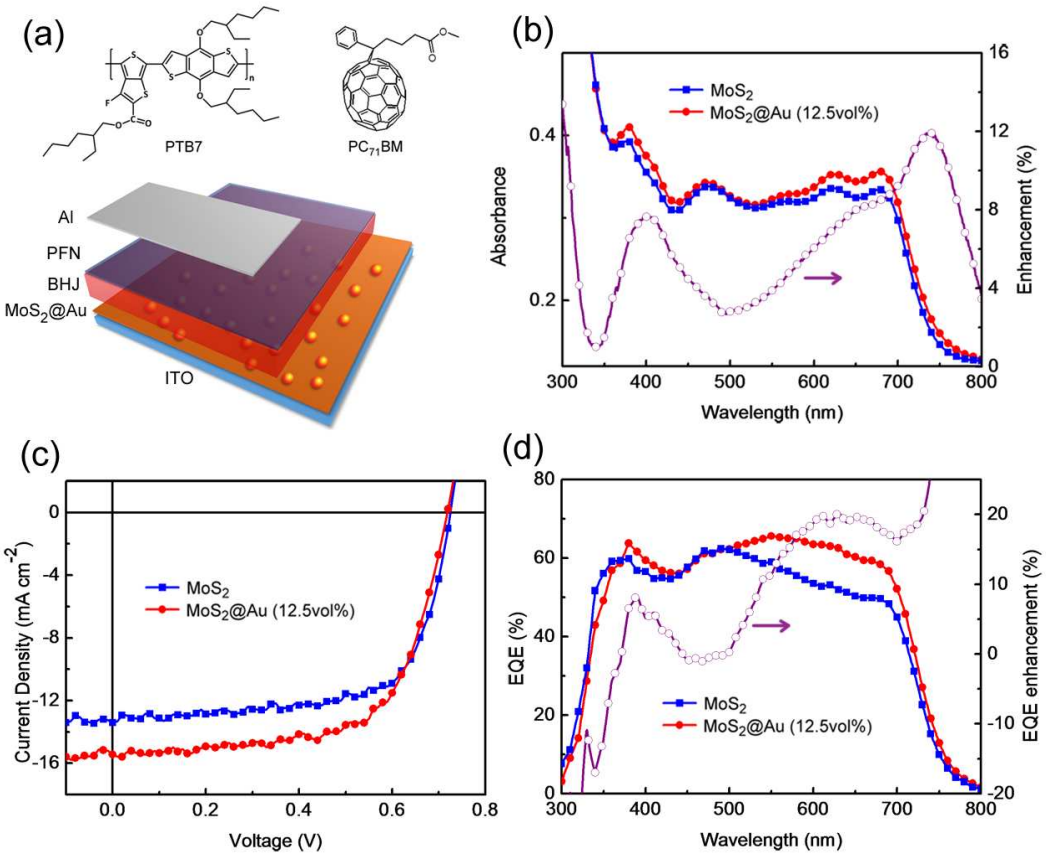

Figure 5. (a) Chemical structures of PTB7 and$PC_{71}BM$ and schematic of the device architecture. Bottom to up: ITO/MoS_2@Au/BHJ/PFN/Al. (b) UV-Vis absorption spectra of PTB7:$PC_{71}BM$ BHJ films with MoS_2 HTL and multi-functional MoS_2@Au HTL (the absorption enhancement after incorporation Au NPs onto MoS_2 sheets is provided). (c) *J-V* characteristics and (d) external quantum efficiency (EQE) spectra of the OSC devices with MoS_2 HTL and MoS_2@Au HTL (12.5*vol*%), under AM 1.5G illumination (100 mW cm^{-2}). The calculated EQE enhancement against wavelength is also presented in (d).

Table 1. Performances of OSCs with MoS_2@Au HTL containing different Au decoration coverages under AM 1.5G illumination (100 $mWcm^{-2}$).

Anode buffer layer	Jsc [mA/cm^2]	Voc [V]	FF	PCE [%]
MoS_2@Au (0 vol%)	13.36±0.30	0.73±0.01	0.634±0.01	6.18±0.20
MoS_2@Au (2.5 vol%)	14.33±0.10	0.73±0.01	0.632±0.02	6.61±0.15
MoS_2@Au (5 vol%)	14.52±0.25	0.72±0.01	0.647±0.01	6.76±0.10
MoS_2@Au (10 vol%)	15.01±0.15	0.72±0.01	0.634±0.03	6.85±0.15
MoS_2@Au (12.5 vol%)	15.44±0.20	0.72±0.01	0.652±0.01	7.25±0.10
MoS_2@Au (15 vol%)	15.33±0.20	0.73±0.01	0.627±0.03	7.02±0.25
MoS_2@Au (20 vol%)	14.33±0.10	0.73±0.01	0.654±0.01	6.84±0.10